We are IntechOpen, the world's leading publisher of Open Access books Built by scientists, for scientists

6,900
Open access books available

186,000
International authors and editors

200M
Downloads

Our authors are among the

154
Countries delivered to

TOP 1%
most cited scientists

12.2%
Contributors from top 500 universities

CLARIVATE ANALYTICS
BOOK CITATION INDEX
INDEXED

WEB OF SCIENCE™

Selection of our books indexed in the Book Citation Index
in Web of Science™ Core Collection (BKCI)

Interested in publishing with us?
Contact book.department@intechopen.com

Numbers displayed above are based on latest data collected.
For more information visit www.intechopen.com

CFD Modelling of Fluidized Bed with Immersed Tubes

A.M.S. Costa, F.C. Colman, P.R. Paraiso and L.M.M. Jorge
Universidade Estadual de Maringa
Brazil

1. Introduction

Fluidized beds are widely used in combustion and chemical industries. The immersed tubes are usually used for enhancement of heat transfer or control of temperature in fluidized beds. By his turn, tubes subjected to the solid particle impact may suffer severe erosion wear. Many investigations have been devoted to erosion in tubes immersed in fluidized beds on the various influencing factors (cf. Lyczkowski and Bouillard, 2002). As pointed by Achim et al. (2002), the factors can be classified as particle characteristics, mechanical design and operating conditions.

Some previous experimental studies have focused on bubble and particle behaviors (Kobayashi et al., 2000, Ozawa et al., 2002), tube attrition, erosion or wastage (Bouillard and Lyczkowski, 1991; Lee and Wang, 1995; Fan et al., 1998; Wiman, 1994), heat transfer (Wong and Seville, 2006, Wiman and Almstedt, 1997) and gas flow regimes (Wang et. al, 2002).

Previous numerical studies were also performed using different CFD codes. Recently He et al. (2009, 2004), using the K-FIX code adapted to body fitted coordinates investigated the hydrodynamics of bubbling fluidized beds with one to four immersed tubes. The erosion rates predicted using the monolayer kinetic energy dissipation model were compared against the experimental values of Wiman (1994) for the two tube arrangement. The numerical values were three magnitudes lower than the experimental ones. Also employing a eulerian-eulerian model and the GEMINI numerical code, Gustavsson and Almstedt (2000, 1999) performed numerical computations and comparison against experimental results (Enwald et. al., 1999). As reported for those authors, fairly good qualitative agreement between the experimental and numerical erosion results were obtained, and the contributions to the erosion from the different fluid dynamics phenomena near the tube were identified.

In the present study, we revisit the phenomena of the immersed tubes in a gas fluidized bed with different immersed tube arrangements employing the eulerian-eulerian two fluid model and the MFIX code. The purposes of the numerical simulations are to compare and explore some effects not previously investigated in the above-mentioned references.

2. Two fluid and erosion model

The mathematical model is based on the assumption that the phases can be mathematically described as interpenetrating continua; the point variables are averaged over a region that is

large compared with the particle spacing but much smaller than the flow domain (see Anderson, 1967). A short summary of the equations solved by the numerical code in this study are presented next. Refer to Benyahia et al. (2006) and Syamlal et al. (1993) for more detailment.

The continuity equations for the fluid and solid phase are given by :

$$\frac{\partial}{\partial t}\left(\varepsilon_f \rho_f\right) + \nabla \bullet \left(\varepsilon_f \rho_f \vec{v}_f\right) = 0 \tag{1}$$

$$\frac{\partial}{\partial t}\left(\varepsilon_s \rho_s\right) + \nabla \bullet \left(\varepsilon_s \rho_s \vec{v}_s\right) = 0 \tag{2}$$

In the previous equations ε_f, ε_s, ρ_f, ρ_s, $\vec{v}_f$ and $\vec{v}_s$ are the volumetric fraction, density and velocity field for the fluid and solids phases.

The momentum equations for the fluid and solid phases are given by:

$$\frac{\partial}{\partial t}\left(\varepsilon_f \rho_f \vec{v}_f\right) + \nabla \bullet \left(\varepsilon_f \rho_f \vec{v}_f \vec{v}_f\right) = \nabla \bullet \overline{\overline{S}}_f + \varepsilon_f \rho_f \vec{g} - \vec{I}_{fs} \tag{3}$$

$$\frac{\partial}{\partial t}\left(\varepsilon_s \rho_s \vec{v}_s\right) + \nabla \bullet \left(\varepsilon_s \rho_s \vec{v}_s \vec{v}_s\right) = \nabla \bullet \overline{\overline{S}}_s + \varepsilon_s \rho_s \vec{g} + \vec{I}_{fs} \tag{4}$$

$\overline{\overline{S}}_f$ $\overline{\overline{S}}_s$ are the stress tensors for the fluid and solid phase. It is assumed newtonian behavior for the fluid and solid phases, i.e.,

$$\overline{\overline{S}} = \left(-P + \lambda \nabla \bullet \vec{v}\right)\overline{\overline{I}} + 2\mu \, S_{ij} \equiv -p \, \overline{\overline{I}} + \overline{\overline{\tau}} \qquad S_{ij} = \frac{1}{2}\left[\nabla \vec{v} + \left(\nabla \vec{v}\right)^T\right] - \frac{1}{3}\nabla \bullet \vec{v} \tag{5a,b}$$

In the above equation P, λ, μ are the pressure, bulk and dynamic viscosity, respectively.

In addition, the solid phase behavior is divided between a plastic regime (also named as slow shearing frictional regime) and a viscous regime (also named as rapidly shearing regime). The constitutive relations for the plastic regime are related to the soil mechanics theory. Here they are represented as:

$$p_s^p = f_1\left(\varepsilon^*, \varepsilon_f\right). \qquad \mu_s^p = f_2\left(\varepsilon^*, \varepsilon_f, \phi\right) \tag{6}$$

In the above equation ε^* is the packed bed void fraction and ϕ is the angle of internal friction.

A detailing of functions f_1 to f_4 and f_9 can be obtained in Benyahia (2008).

On the other hand, the viscous regime behavior for the solid phase is ruled by two gas kinetic theory related parameters (e, Θ).

$$p_s^v = f_3\left(\varepsilon_s, \rho_s, d_p, \Theta, e\right) \qquad \mu_s^v = f_4\left(\varepsilon_s, \rho_s, d_p, \Theta^{1/2}, e\right) \tag{7}$$

The solid stress model outlined by Eqs. (6) and (7) will be quoted here as the standard model. Additionally, a general formulation for the solids phase stress tensor that admits a transition between the two regimes is given by :

$$\overline{\overline{S}}_s = \begin{cases} \phi(\varepsilon_f)\overline{\overline{S}}_s^v + \left[1-\phi(\varepsilon_f)\right]\overline{\overline{S}}_s^p & \text{if } \varepsilon_f < \varepsilon^* + \delta \\ \overline{\overline{S}}_s^v & \text{if } \varepsilon_f \geq \varepsilon^* + \delta \end{cases} \tag{8}$$

According to Pannala et al.(2009), two diferent formulations for the weighting parameter "ϕ" can be employed :

$$\phi(\varepsilon) = \frac{1}{1 + \upsilon^{\frac{\varepsilon-\varepsilon^*}{2\delta\varepsilon^*}}} \qquad \phi(\varepsilon) = \frac{\text{Tanh}\left(\frac{\pi\left(\varepsilon-\varepsilon^*\right)}{\delta\varepsilon^*}\right)+1}{2} \tag{9a,b}$$

In the above equation the void fraction range δ and the shape factor υ are smaller values less than unity. It must be emphasized that when δ goes to zero and ϕ equals to unity, the "switch" model as proposed by Syamlal et al. (1993) based on the Schaeffer (1987) can be recovered. The models based on eqs. (9a) and (9b) will be referred in the numerical simulations as BLEND S and BLEND T, respectivelly.

On the other hand, the Srivastava and Sundaresan (2003), also called "Princeton model", can be placed on the basis of Eq. (9)

Also in equations (4) and (5) $\vec{I}_{fs}$ is the momentum interaction term between the solid and fluid phases, given by

$$\vec{I}_{fs} = -\varepsilon_s \nabla P_f - \beta\left(\vec{v}_s - \vec{v}_f\right) \tag{10}$$

There is a number of correlations for the drag coefficient β (Eqs. 11 to 16). The first of the correlations for the drag coefficient is based on Wen and Yu (1966) work. The Gidaspow drag coefficient is a combination between the Wen Yu correlation and the correlation from Ergun (1952). The Gidaspow blended drag correlation allows controlling the transition from the Wen and Yu, and Ergun based correlations. In this correlation the χ blending function was originally proposed by Lathowers and Bellan (2000) and the value of parameter C controls the degree of transition. From Eq. (14), the correlation proposed by Syamlal and O'Brien (1993) carries the advantage of adjustable parameters C_1 and d_1 for different minimum fluidization conditions. The correlations given in Eq. (15) and Eq. (16) are based on Lattice-Boltzmann simulations. For detailments of these last drag correlations refer to the works by Benyahia et al. (2006) and Wang et al. (2010).

$$\beta_{\text{Wen-Yu}} = \frac{3}{4}C_D \frac{\rho_f \varepsilon_f \varepsilon_s \left|\vec{v}_f - \vec{v}_s\right|}{d_p} \varepsilon_f^{-2.65}$$

$$C_D = \begin{cases} \frac{24}{\text{Re}}\left(1+0.15\text{Re}^{0.687}\right) & \text{Re}<1000 \\ 0.44 & \text{Re} \geq 1000 \end{cases} \qquad \text{Re} = \frac{\rho_f \varepsilon_f \left|\vec{v}_f - \vec{v}_s\right| d_p}{\mu_f} \tag{11}$$

$$\beta_{\text{Gidaspow}} = \begin{cases} \beta_{\text{Wen-Yu}} & \varepsilon_f > 0.8 \\ \beta_{\text{Ergun}} = \dfrac{150\,\varepsilon_s\left(1-\varepsilon_s\right)\mu_f}{\varepsilon_f d_p^2} + \dfrac{1.75\,\rho_f \varepsilon_s \left|\vec{v}_f - \vec{v}_s\right|}{d_p} & \varepsilon_f \leq 0.8 \end{cases} \tag{12}$$

$$\beta_{\text{Gidaspow-blended}} = \chi\,\beta_{\text{Wen-Yu}} + \left(1-\chi\right)\beta_{\text{Ergun}} \qquad \chi = \dfrac{\tan^{-1}\left(C\left(\varepsilon_f - 0.8\right)\right)}{\pi} + 0.5 \tag{13}$$

$$\beta_{\text{Syamlal-OBrien}} = \frac{3}{4}\frac{\rho_f \varepsilon_f \varepsilon_s}{V_r^2 d_p}\left(0.63 + 4.8\sqrt{\frac{V_r}{\text{Re}}}\right)^2 \left|\vec{v}_f - \vec{v}_s\right|$$

$$V_r = 0.5A - 0.03\,\text{Re} + 0.5 \times \sqrt{\left(0.06\,\text{Re}\right)^2 + 0.12\,\text{Re}\left(2B-A\right) + A^2} \tag{14}$$

$$A = \varepsilon_f^{4.14} \qquad B = \begin{cases} C_1 \varepsilon_f^{1.28} & \varepsilon_f \leq 0.85 \\ \varepsilon_f^{d_1} & \varepsilon_f > 0.85 \end{cases}$$

$$\beta_{\text{Hill-Koch-Ladd}} = 18\mu_f\left(1-\varepsilon_s\right)^2 \varepsilon_s \frac{F}{d_p^2} \qquad F = f_9\left(F_0, F_1, F_2, F_3\right) \tag{15}$$

$$\beta_{\text{Beestra}} = 180\frac{\mu_f \varepsilon_s^2}{d_p^2} + 18\frac{\mu_f \varepsilon_f^3 \varepsilon_s\left(1+1.5\sqrt{\varepsilon_s}\right)}{d_p^2} + 0.31\frac{\mu_f \varepsilon_s\,\text{Re}}{\varepsilon_f d_p^2}\frac{\left[\varepsilon_f^{-1} + 3\varepsilon_f \varepsilon_s + 8.4\,\text{Re}^{-0.343}\right]}{\left[1+10^{3\varepsilon_s}\,\text{Re}^{-0.5-2\varepsilon_s}\right]} \tag{16}$$

For closing the model, a transport equation for the granular energy Θ provides a way of determine the pressure and viscosity for the solid phase during the viscous regime. Equation (17) is a transport equation for the granular energy Θ. Its solution provides a way of determine the pressure and viscosity for the solid phase during the viscous regime. The terms κ_s γ and ϕ_{gs} are the granular energy conductivity, dissipation and exchange, respectively.

$$\frac{3}{2}\left[\frac{\partial}{\partial t}\varepsilon_s \rho_s \Theta + \nabla \cdot \rho_s \vec{v}_s \Theta\right] = \bar{\bar{S}}_s : \nabla \vec{v}_s - \nabla \cdot \left(\kappa_s \nabla \Theta\right) - \gamma + \phi_{gs} \tag{17}$$

$$\kappa_s = f_5\left(\varepsilon_s, \rho_s, d_p, \Theta^{1/2}, e, \beta\right)$$

$$\gamma = f_6\left(\varepsilon_s, \rho_s, d_p, \Theta^{3/2}, e\right) \tag{18}$$

$$\phi_{gs} = f_7\left(\varepsilon_s, \rho_s, d_p, \Theta, \left|\vec{v}_f - \vec{v}_s\right|, \beta\right)$$

In the algebraic approach, instead solving the full equation (17) , the granular energy is obtained by equating the first term on the right hand side with the dissipation term.

The model where Eqs. (5) to (8) and (17) are solved is the kinetic theory model, termed here as KTGF. Conversely, in the constant solids viscosity model (CVM) the solids pressure is defined as in Eq. (6) and the solids viscosity in either plastic and viscous regimes is set equal to a constant.

For erosion calculations in this work we use the monolayer energy dissipation model (Lyczkowski and Bouillard, 2002). In that model the kinetic energy dissipation rate for the solids phase in the vicinity of stationary immersed surfaces is related to erosion rate in m/s by multiplication with an appropriate constant. This constant is function of surface hardness, elasticity of collision and diameter of particles hitting the surface. The kinetic energy dissipation rate Φ_s in W/m^3 for the solids phase is given by :

$$\Phi_s = \left[\varepsilon_s \overline{\overline{\tau}}_s : \nabla \vec{v}_s + \beta \frac{\vec{v}_s^2}{2} \right] \tag{19}$$

3. Numerical method

MFIX (Multiphase Flow with Interphase eXchanges) is an open source CFD code developed at the National Energy Technology Laboratory (NETL) for describing the hydrodynamics, heat transfer and chemical reactions in fluid-solids systems. It has been used for describing bubbling and circulating fluidized beds, spouted beds and gasifiers. MFIX calculations give transient data on the three-dimensional distribution of pressure, velocity, temperature, and species mass fractions.

The hydrodynamic model is solved using the finite volume approach with discretization on a staggered grid. A second order accurate discretization scheme was used and superbee scheme was adopted for discretization of the convective fluxes at cell faces for all equations in this work. With the governing equations discretized, a sequential iterative solver is used to calculate the field variables at each time step. The main numerical algorithm is an extension of SIMPLE. Modifications to this algorithm in MFIX include a partial elimination algorithm to reduce the strong coupling between the two phases due to the interphase transfer terms. Also, MFIX makes use of a solids volume fraction correction step instead of a solids pressure correction step which is thought to assist convergence in loosely packed regions. Finally, an adaptive time step is used to minimize computation time. See Syamlal (1998) for more details. The immersed obstacles were implemented using the cut-cell technique available in the code (Dietiker, 2009)

The numerical runs were based on experiments of Wiman (1994, 1997) in an air pressurized bed with horizontal tubes for four different tube-bank geometries. The T2 and I4 are portrayed in Fig. 1 whereas the S4 and S4D tubes geometry are given in Figure 3. Figure 2 details the domain for the numerical simulations and circumferential angle coordinate for erosion measurement. In Fig. 2a is detailed the mesh for the T2 arrangement This non-uniform stretched grid, follows Cebeci et al. (2005) approach, has fine spacing close to the surface of the tubes and coarse spacing away from the surface. For all the other arrangements the mesh was uniform as depicted in Fig. 2b. The mesh employed for the bed without tube, and the I4 arrangement was 60 × 260 cells, and for the S4 and S4D arrangement 60 × 340. The bed was operated at room temperature (24 C) at pressures between 0.1 and 1.6 MPa and at two different excess velocities: $U_{fl} - U_{mf} = 0.2$ m/s and $U_{fl} - U_{mf} = 0.6$ m/s. Here, U_{fl} is the superficial fluidization velocity based on the free bed cross-section. The voidage at minimum fluidization was 0.46 and the minimum fluidization velocities was 0.42 , 0.31 and 0.18 m/s, for 0.1, 0.4 and 1.6 MPa pressures, correspondingly. The particle diameter and density were 700 μm and 2600 kg/m^3. The bubble parameters
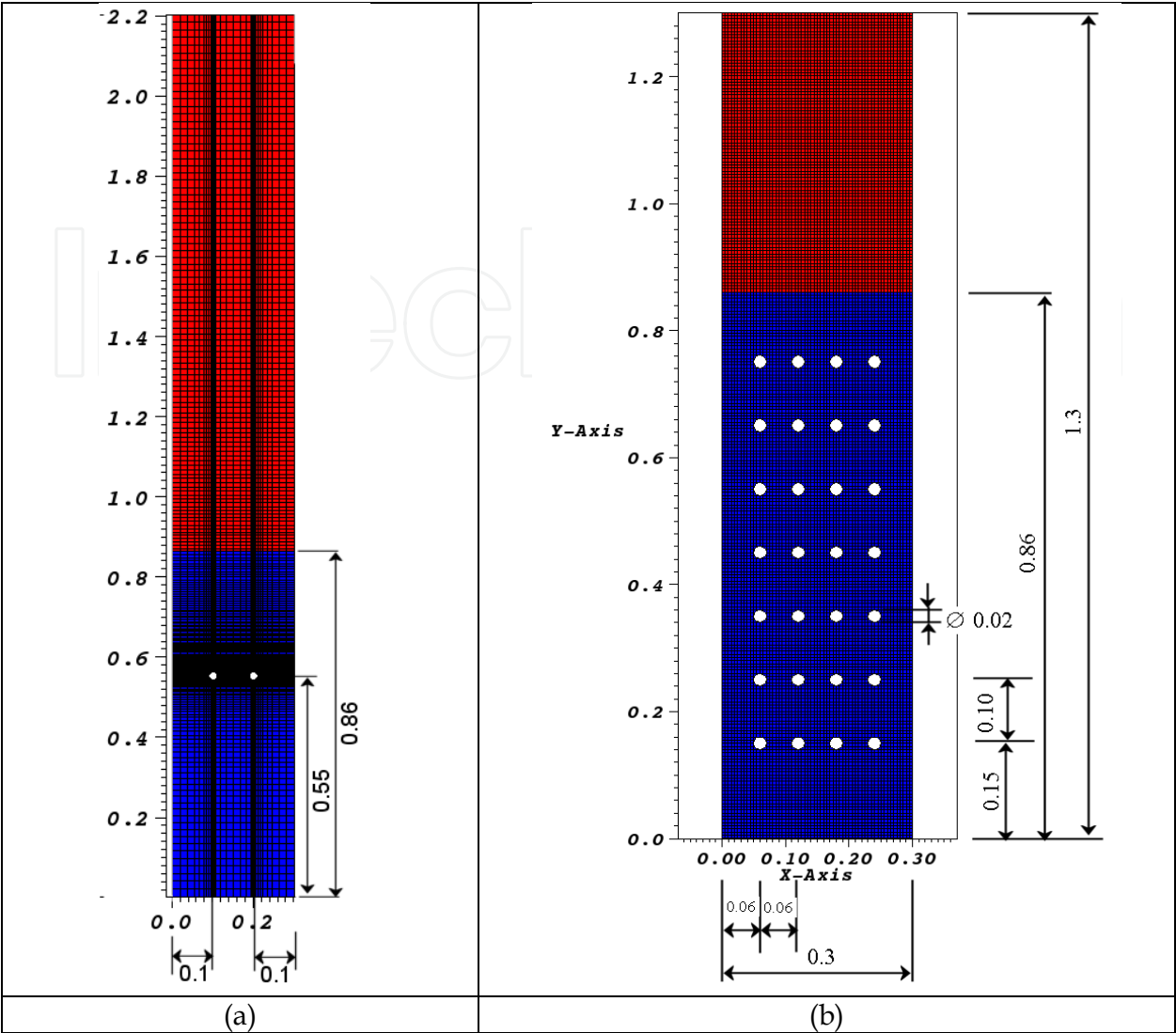
Fig. 1. Geometry and mesh for T2 and I4 tube arrangement.
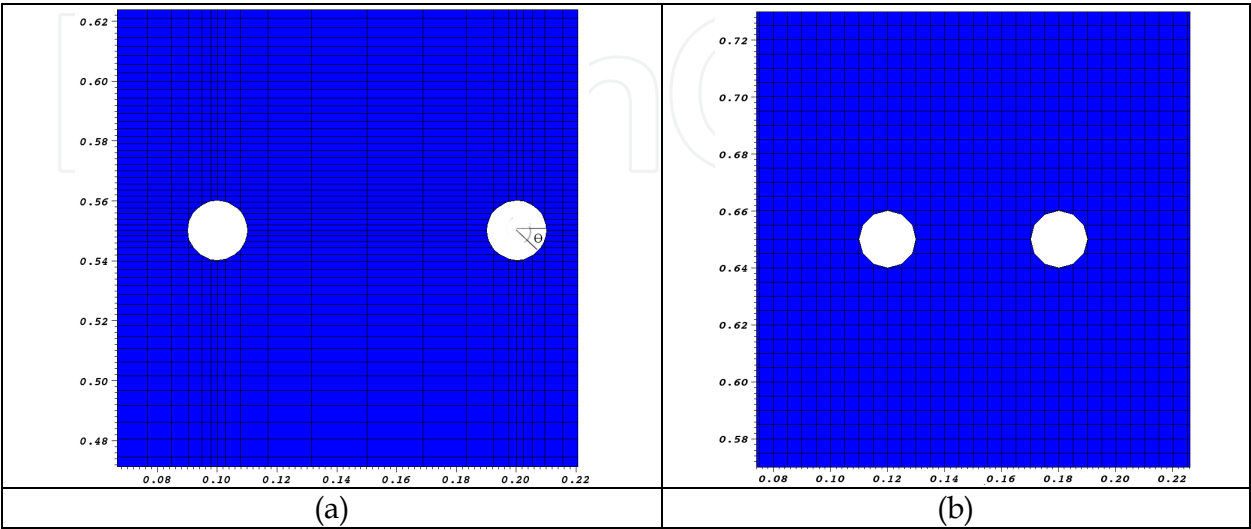

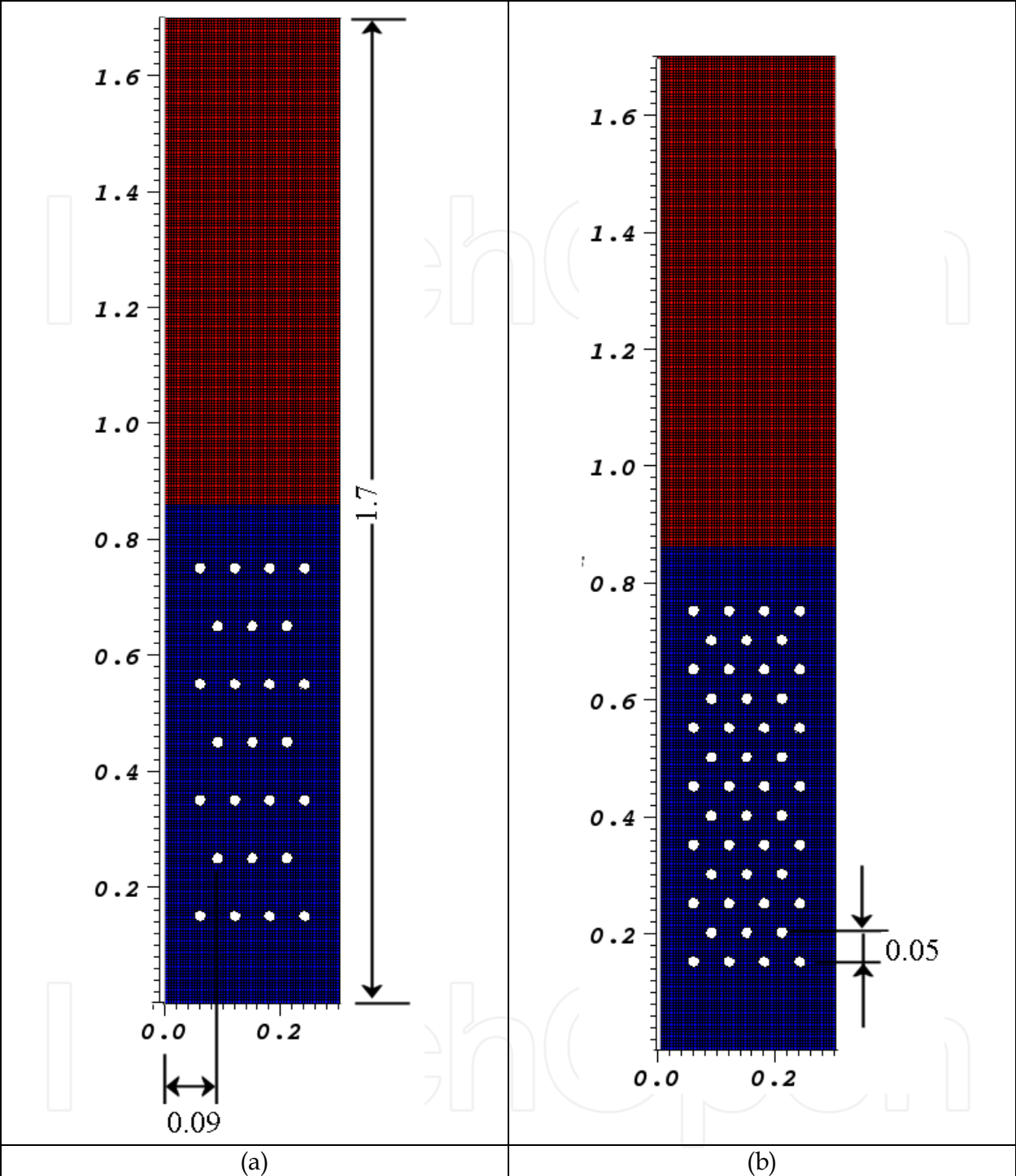Fig. 2. Mesh detailment for (a) T2 arrangement (b) all the others arrangement

Fig. 3. Geometry and mesh for (a) S4 and (b) S4D tube arrangement

obtained from simulation were based on methodology described in Almstedt (1987), using numerical probes in the domain, centered at (0.15, 0.55) and separated from 15 mm. The target tube for erosion measurements is the one centered at (0.18, 0.55) for all the tube arrangements. More information about the experiments can be accessed from Wiman (1994, 1997).

In this work, the parameters for controlling the numerical solution (e.g., under-relaxation, sweep direction, linear equation solvers, number of iterations, residual tolerances) were kept

as their default code values. Moreover, for setting up the mathematical model, when not otherwise specified the code default values were used. The computer used in the numerical simulations was a PC with OpenSuse linux and Intel Quad Core processor. The simulation time was 20 s.

For generating the numerical results, e employed the parameters listed above, referred here as baseline simulation. In addition, for the baseline simulation we employed the Syamlal-O´Brien drag model, the standard solid stress model, and slip and non-slip condition for solid and gas phase, correspondingly. The previous set of models will be referred in the result's section as baseline simulation models.

4. Results and discussion

Figure 4 is a sampling plot showing the instantaneous solids velocities and gas volumetric fraction fields following two different bubbles passage around the obstacle. Analysis of Fig. (4) shows the bubble splitting mechanism taking place and the characteristic time scale for the bubble passage. After the bubble passage, the solid wake has higher solid velocity magnitude around the obstacle. The solids upward movement following the bubble wake and wall downward movement is kept unchanged. Generally, for beds without internal obstacles, bubble size increases with bed height, particle size and superficial velocity. Analysis of CFD results shows that the presence of tubes was found to alter such general trends for bubble growth.

(c) 11 s   (d) 12 s
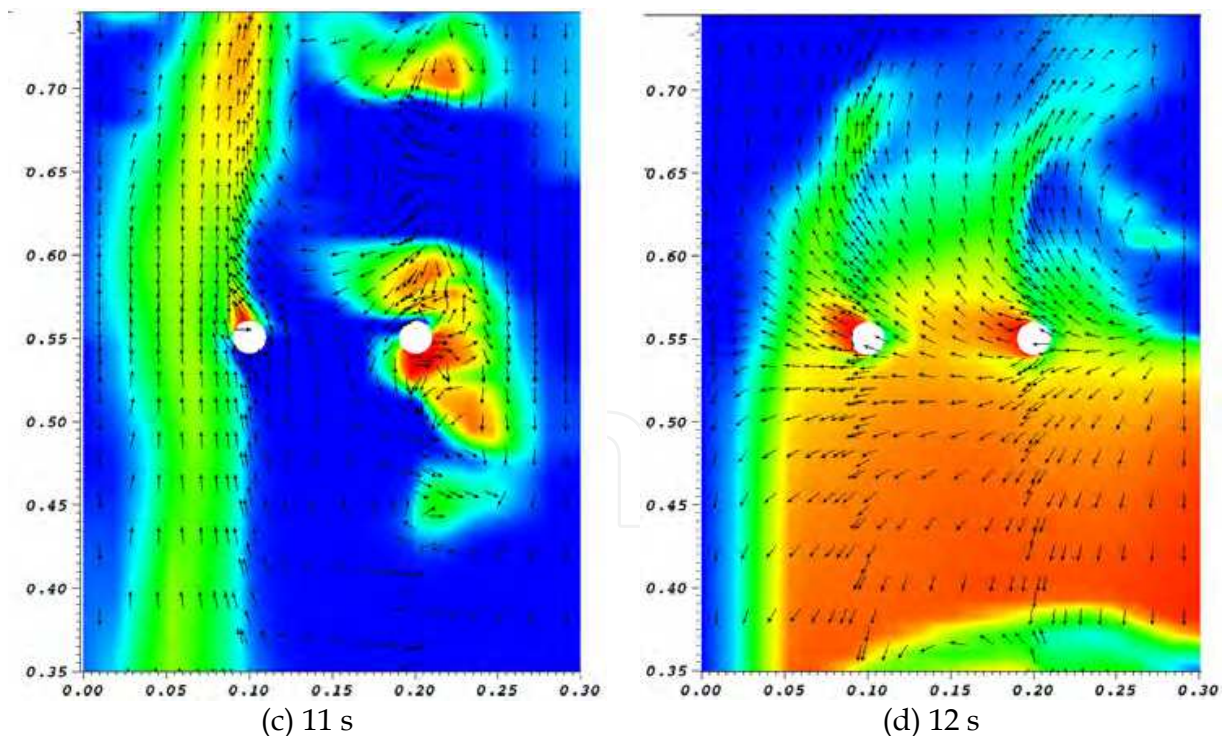
Fig. 4. Detail of the instantaneous voidage and solids velocity vector field for the T2 arrangement

Figure 5 presents the time averaged kinetic energy dissipation as a function of circumferential position θ on the tube surface. As it would be seen from the majority of
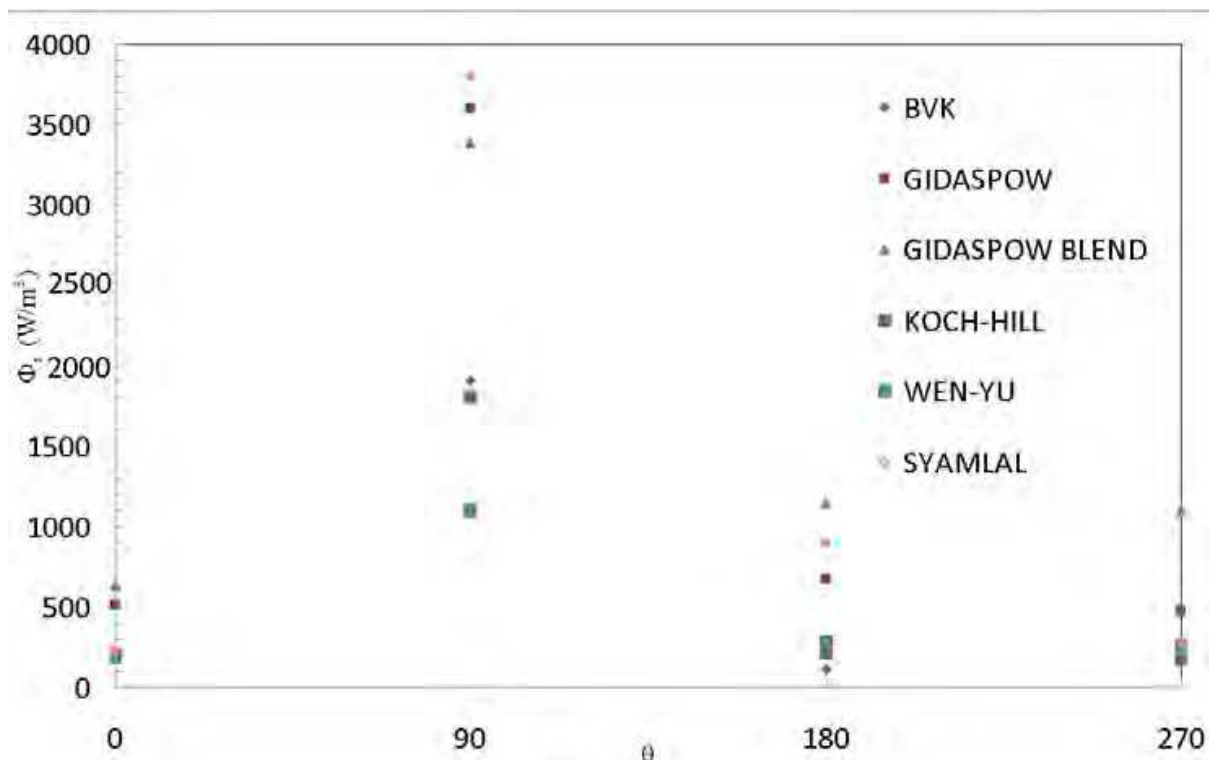
Fig. 5. Time averaged kinetic energy dissipation predicted for different gas-solid drag models – T2 arrangement

results the most severe dissipation occurs on the lower parts of the tube for an angle corresponding to 90 degrees. This fact is in agreement with experimental measured values of erosion from Wiman (1994). Analysis of results shows that, except for the BVK drag model, all the drag models predict the highest dissipation rate occurring at 90 degrees. The value predicted using the Syamlal-O'Brien drag model is the highest. There is a noticeable difference in the value of dissipation value between the Gidaspow and Gidaspow blend drag models, whereas the results by the Wen-Yu drag locate in the intermediate range. By his turn, the results by HYS and Koch-Hill models locates near the Wen-Yu values.

Also, analysis of transient simulated results shows the highest values of kinetic energy dissipation rate occur when the particle fraction suddenly changes from a low to a high value, which corresponds to the tube being hit by the wake of a bubble.

Figure 6 presents the result of kinetic energy dissipation for different solid stress models. As shown the peak values of the dissipation rate are close to 180 degrees for the model with (baseline) and without the blending function discussed in section 2. On the other hand, the maximum value predicted by the constant solids viscosity model (NO KTGF) locates around 180 degrees, and it is superior to the predicted by the solids kinetic energy theory.

Figure 7 presents the result of kinetic energy dissipation for different tube surface slip conditions. The baseline case considers the free slip condition for the solids and non-slip condition for the gas. The peak values do not change when considering the solids with the non-slip condition. On the other hand, when considering slip conditions for both phases the value decreased. The above results, suggests the free slip condition for the gas phase
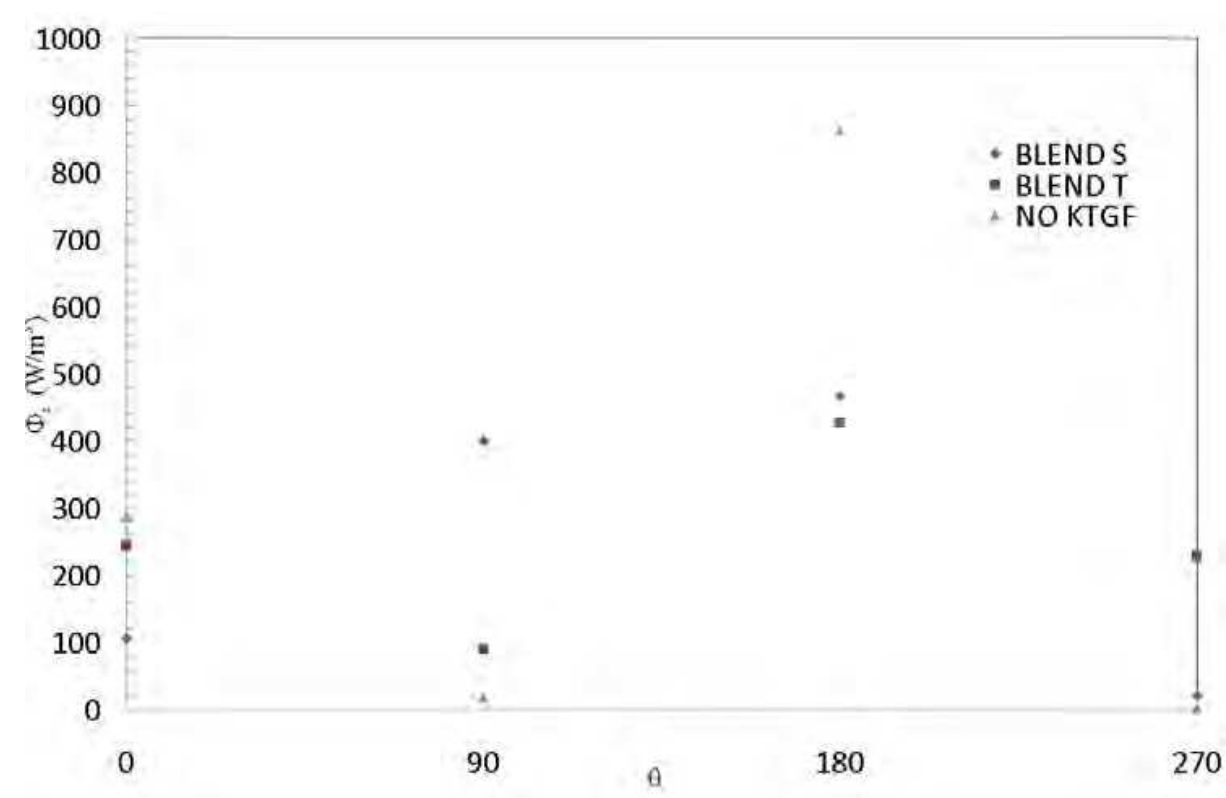
Fig. 6. Time averaged kinetic energy dissipation predicted for different solid stress models
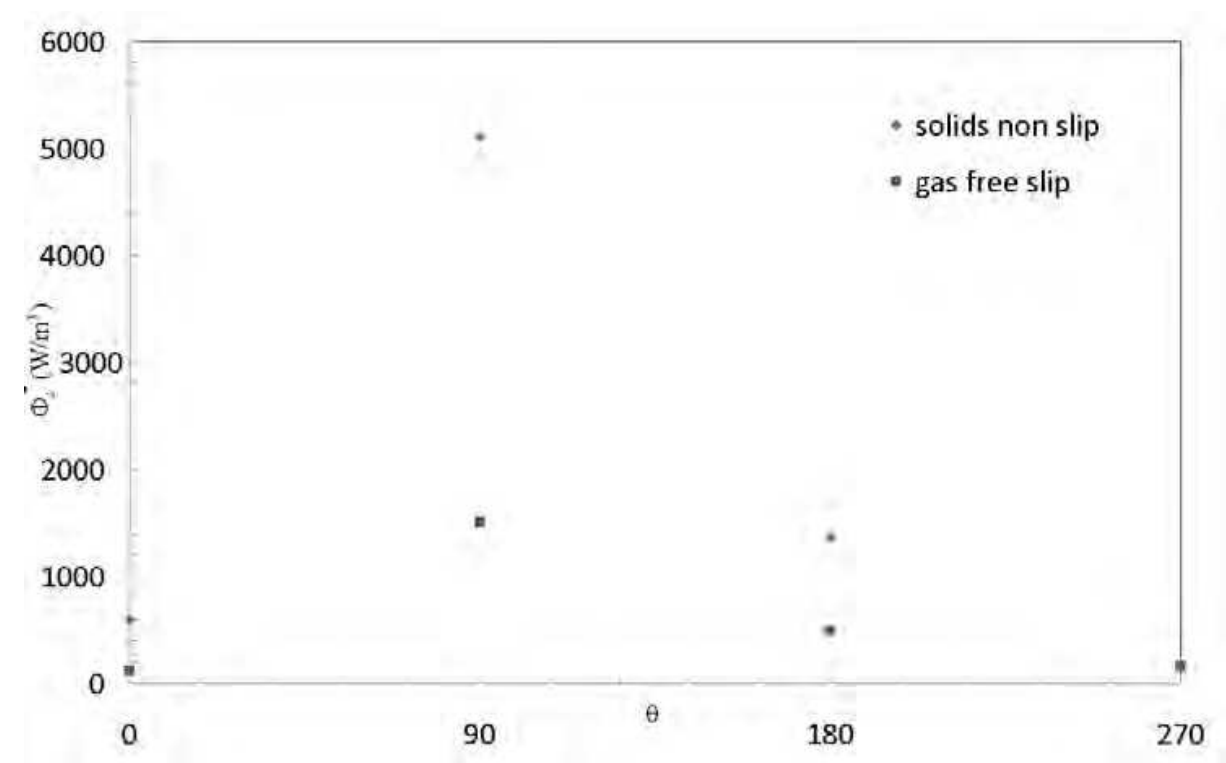

Fig. 7. Time averaged kinetic energy dissipation predicted for different tube surface slip conditions

on the surface of the tube plays an important role on the value of the kinetic energy dissipation.

Figures 8 and 9 shows a comparison between the numerically predicted time averaged values of the kinetic energy dissipation rate, using the baseline simulation models discussed in section 2, and those based on the experimental values for the T2 arrangement in the work of Gustavson and Almstedt (2000). A comparison of the numerical and experimental results for the two different operational pressures (c.f. Figs 8 and 9) shows some degree of discordance. However, the lack of minutely agreement with experimental values, the results can be compared for recognizing similar drifts. For instance, from the Fig 8, the higher simulated values of the dissipation rate occurring in the bottom position of the tube, i.e. for $\theta < 180^{\circ}$, is in agreement with the experimental counterpart. Similarly, the increase of dissipation rate with increased operational pressure for the simulated results is in agreement with the experimental values. Regarding the erosion and baseline models used for the simulation, some remarks towards better agreement with experimental values can also be done. According to the monolayer erosion model and its discussion above Eq. (19) some degree of uncertainty is associated to the multiplying constant, as the exact value of elasticity of collision is not known. It is also expected, that adjustments in the baseline simulation models, such as those outlined in Figs. (5) to (7) would produce better agreement.

Figure 10 is a sampling plot showing the instantaneous gas volumetric fraction fields for different tube arrangements. Analysis of Fig. (10) shows the influence of immersed obstacles on the bubble splitting mechanism taking place and the bubble passage pattern. Above the tube bank, the bubble appears to grow to size similar to the without tube geometry. For the geometry with tubes the bubble encompasses the obstacles but not at the full width of the bed. The interaction is stronger for the denser tube geometry.

Figures 11 and 12 shows a comparison between the numerically predicted values of bubble frequency, using the baseline simulation models discussed in section 2, and those based on the experimental measurements from the works of Almstedt (1987) and Wiman (1995). As shown in the Fig. 10, the calculated values of N_b are underestimated at higher pressures, while at low pressures, there is a quite good agreement between calculated and experimental results. This conclusion holds true both for the I4 and for the S4D tube arrangement. As in the experimental results there are no noticeable differences for the two tubes arrangements.

Figures 13 and 14 shows a comparison for the bubble frequency for the bed without tube and with the S4 arrangement. As shown in Fig. 13 for the bed without tubes the trend points to a frequency agreement between 0.4 and 0.6 MPa. Up this range the values differences increases as pressures increases up to 1.6 MPa. For the S4 arrangement the trend is similar to the I4 and S4D arrangement. The experimental results depicted in Figs. 11 to 14 suggest that the frequency increases with pressure both with and without tubes. For numerical results this holds true only for low pressures, i.e., 0.1 and 0.4 MPa. The numerical results suggest a maxima occurring between 0.4 and 1.6 MPa. On the other hand, the numerical results corroborate the experimental trend that the mean frequency is higher for the bed with tubes than for the freely bubbling bed.
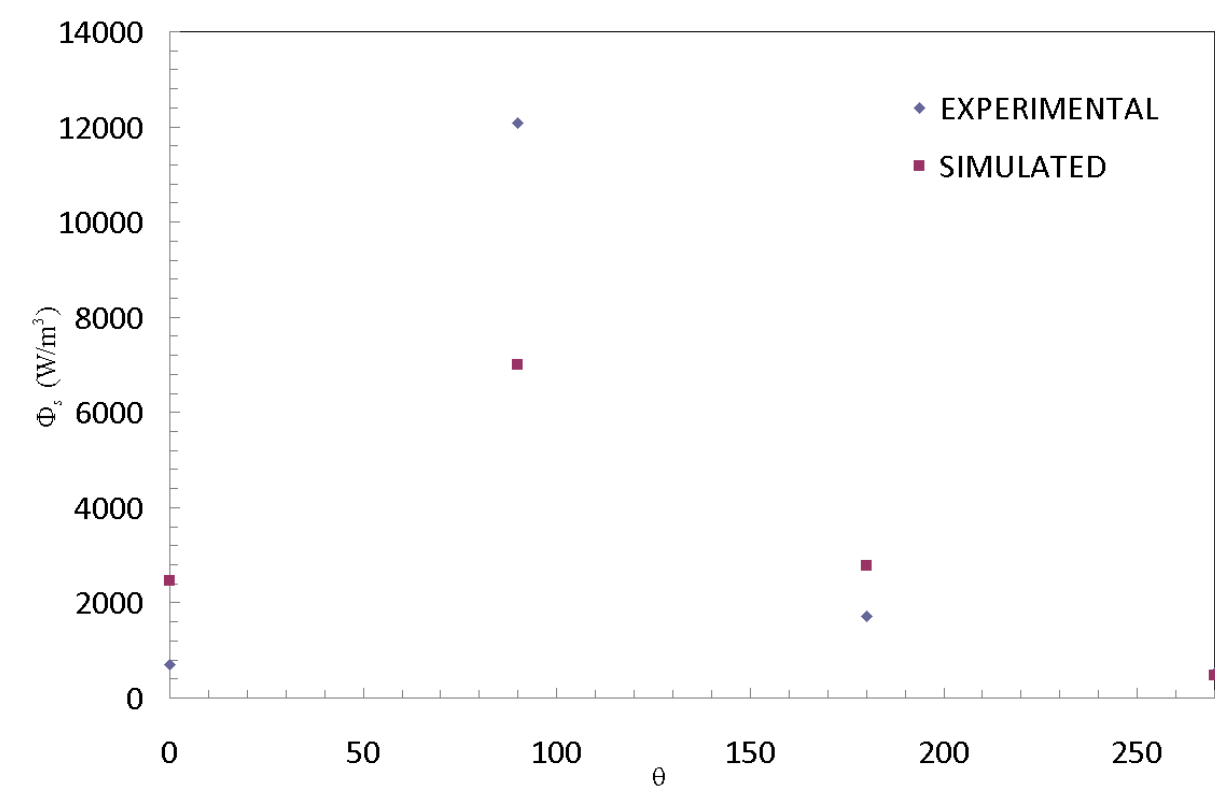
Fig. 8. Simulated kinetic energy dissipation at various circumferential angular positions in the surface of the tube and values from experimental results by Gustavsson and Almstedt, 2000. Operational pressures : 0.8 MPa ;
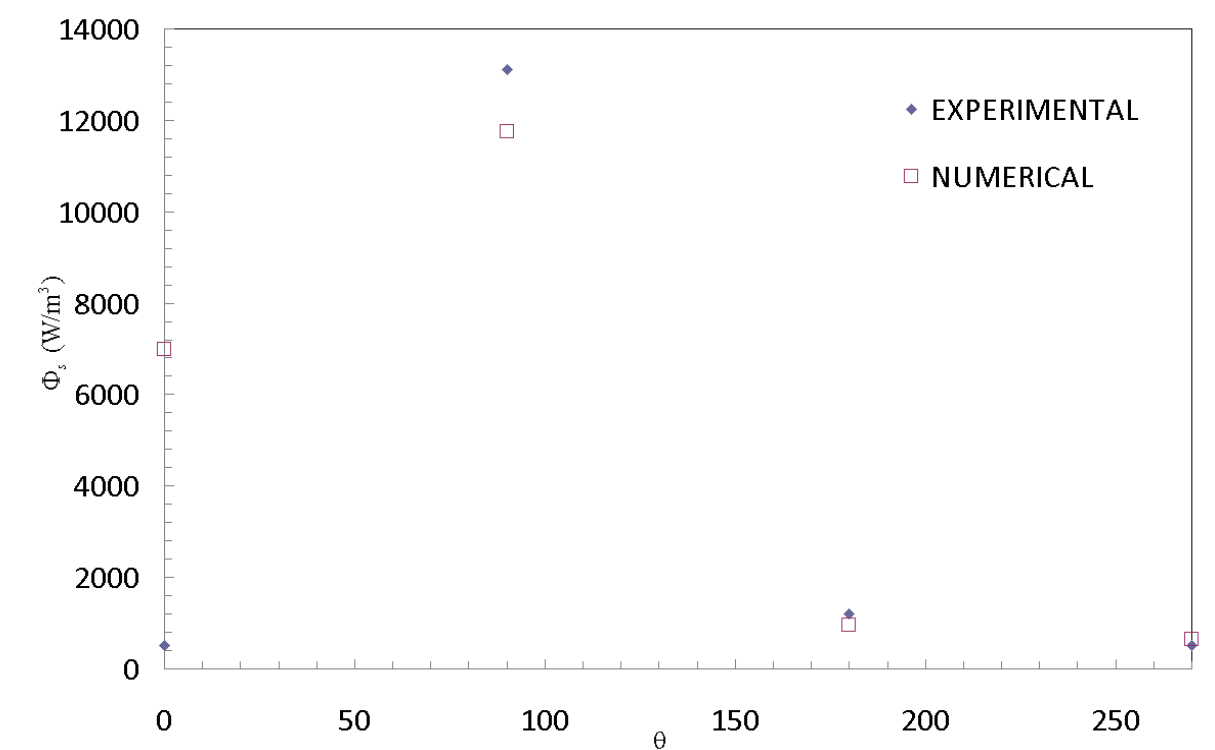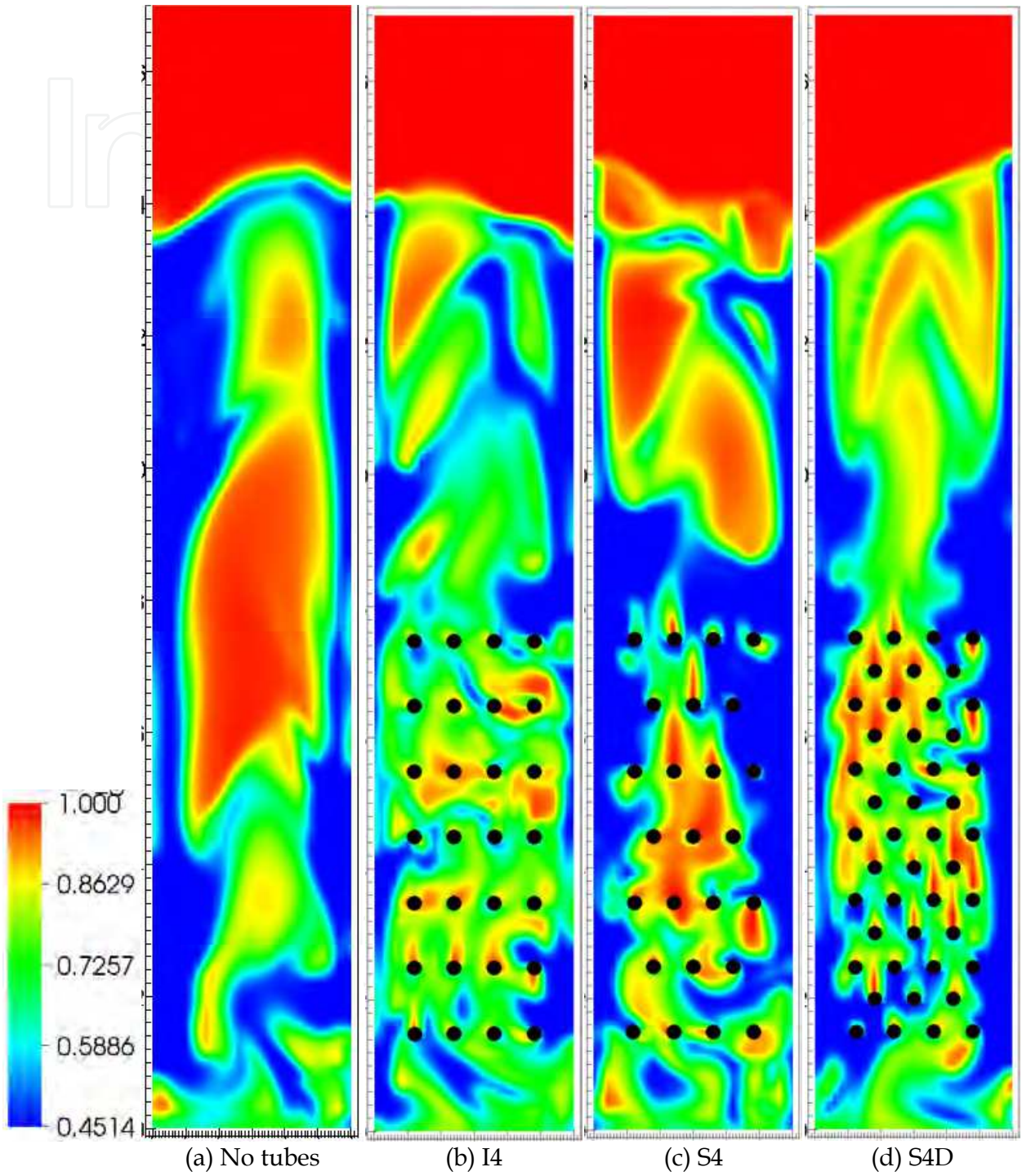

Fig. 9. Simulated kinetic energy dissipation at various circumferential angular positions in the surface of the tube and values from experimental results by Gustavsson and Almstedt, 2000. Operational pressures : 1.6 MPa

Fig. 10. Snapshots of voidage field at 4 s for different tube arrangements. P = 0.4 MPa , Uf = 0.6 m/s
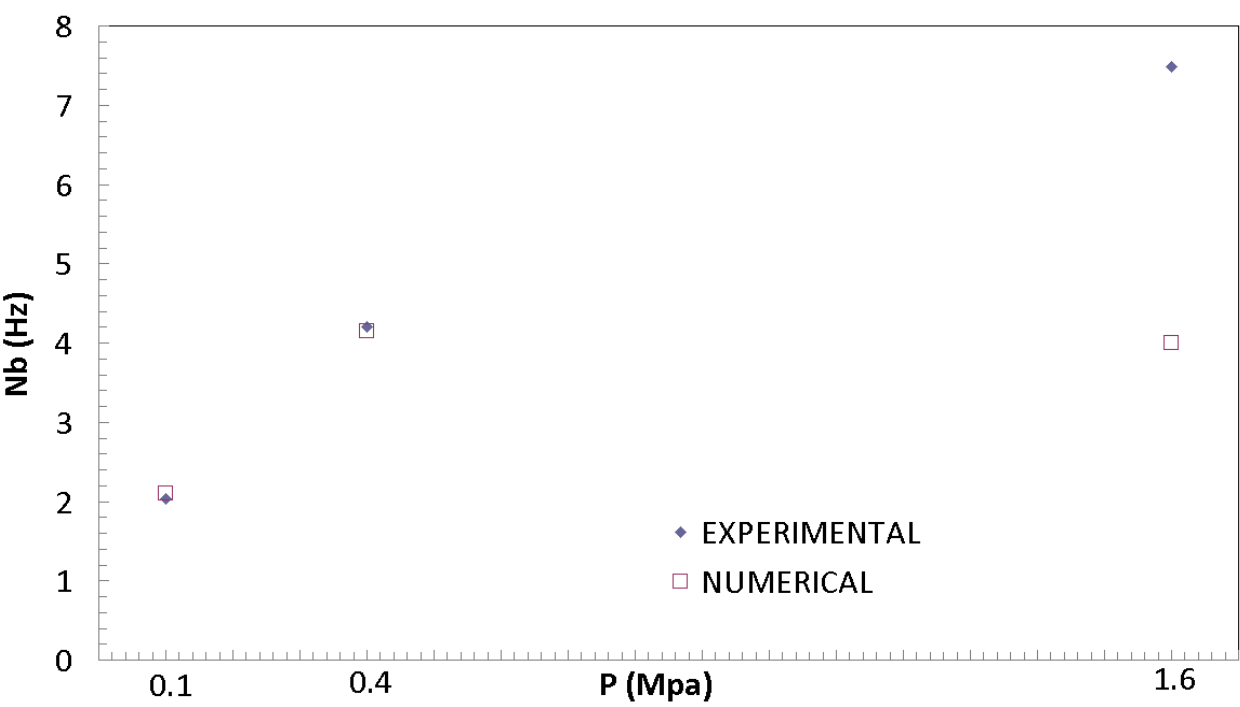
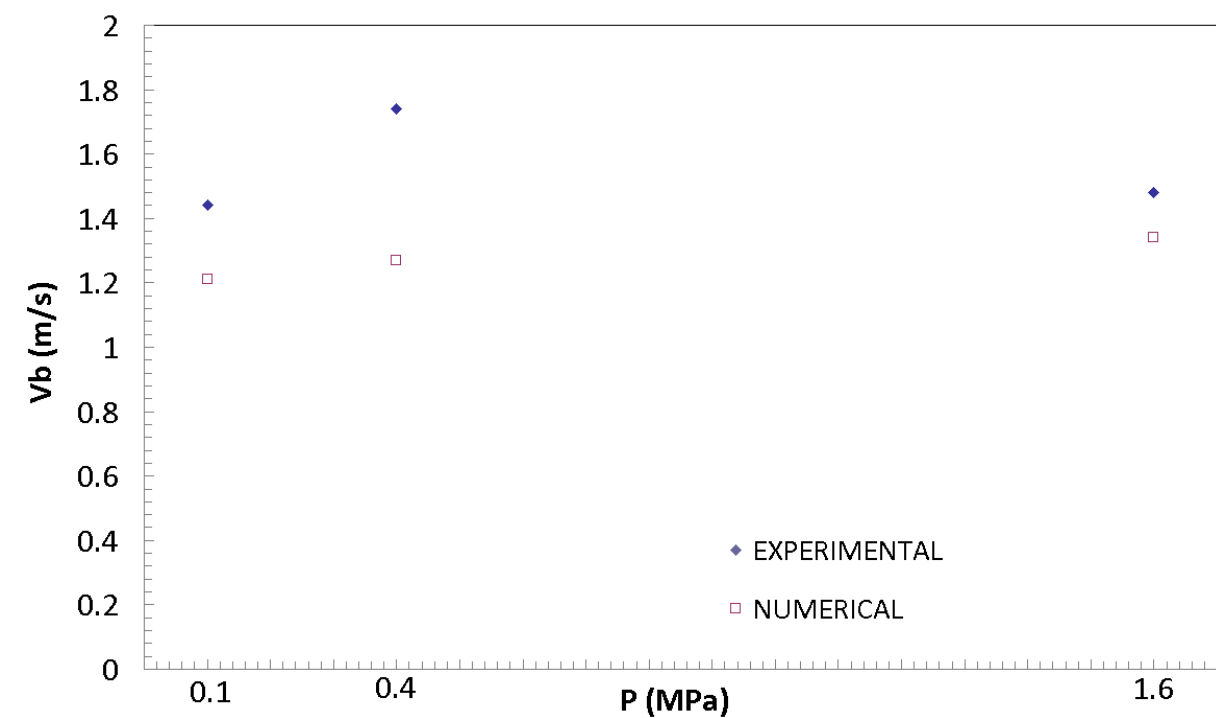Fig. 11. Nb versus pressure, numerical X experimental: I4 arrangement, U_f = 0.6 m/s
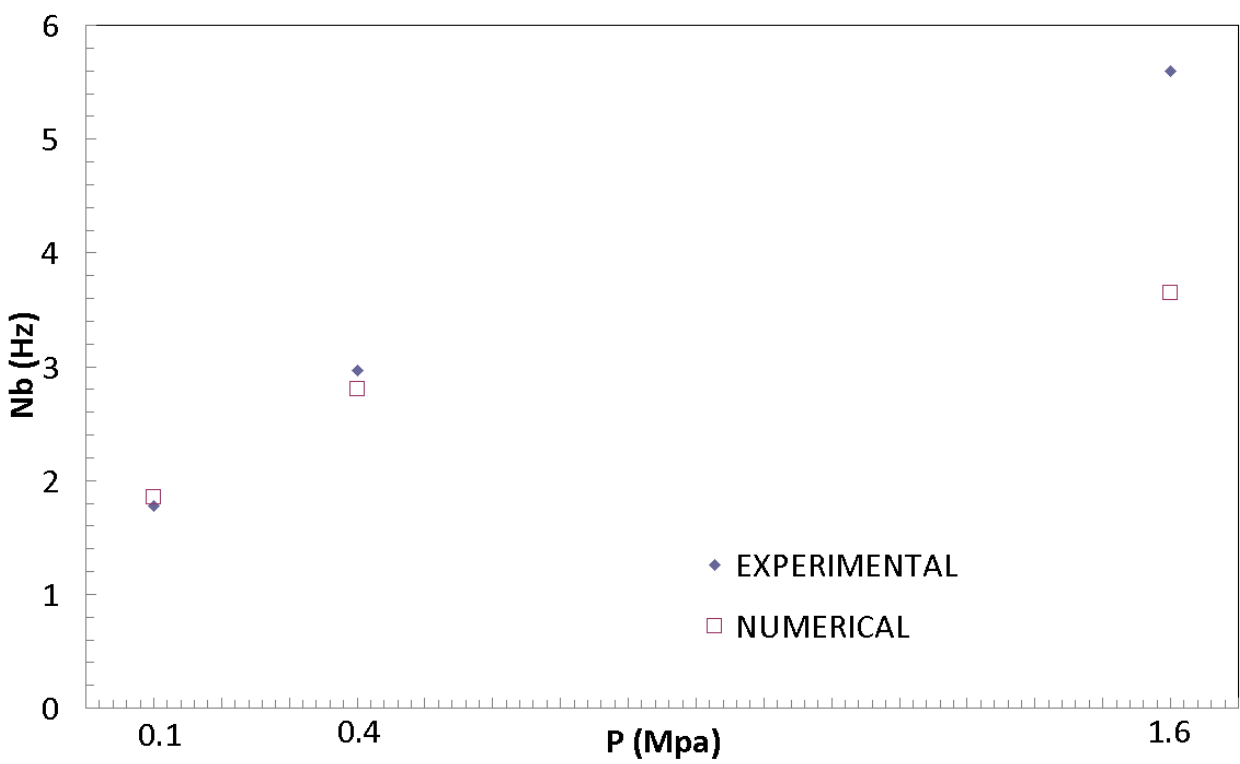
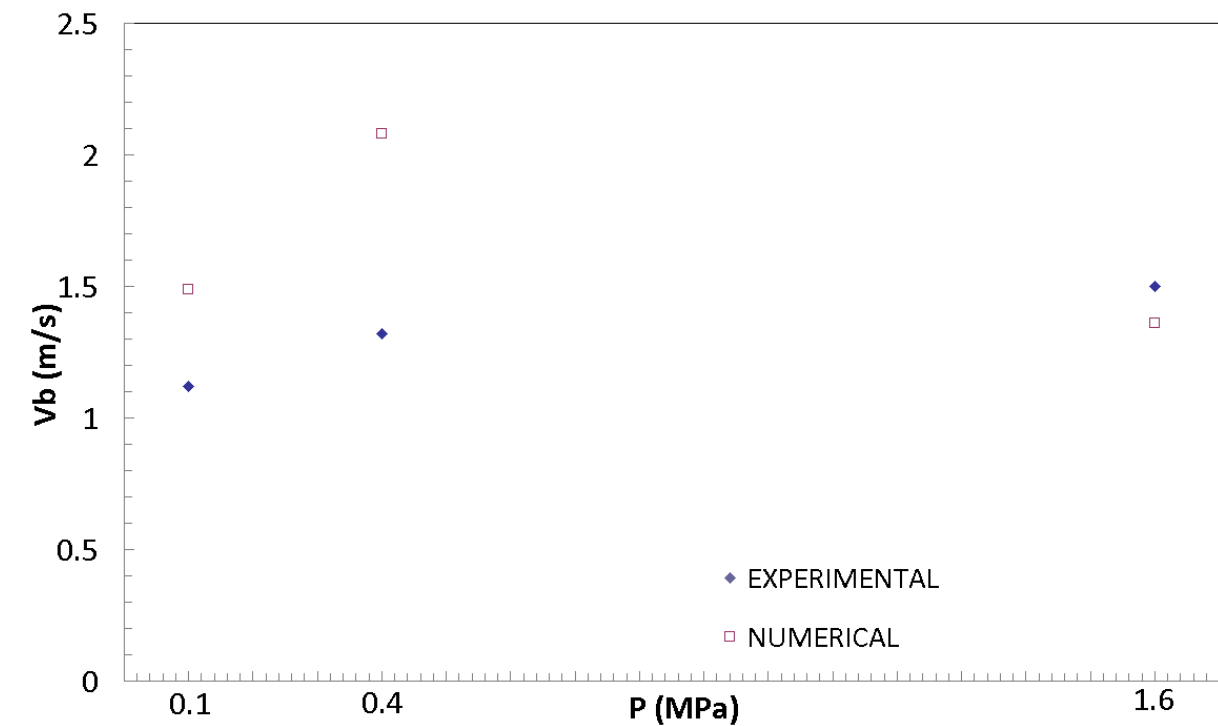Fig. 12. Nb versus pressure, numerical X experimental: S4D arrangement, U_f = 0.6 m/s
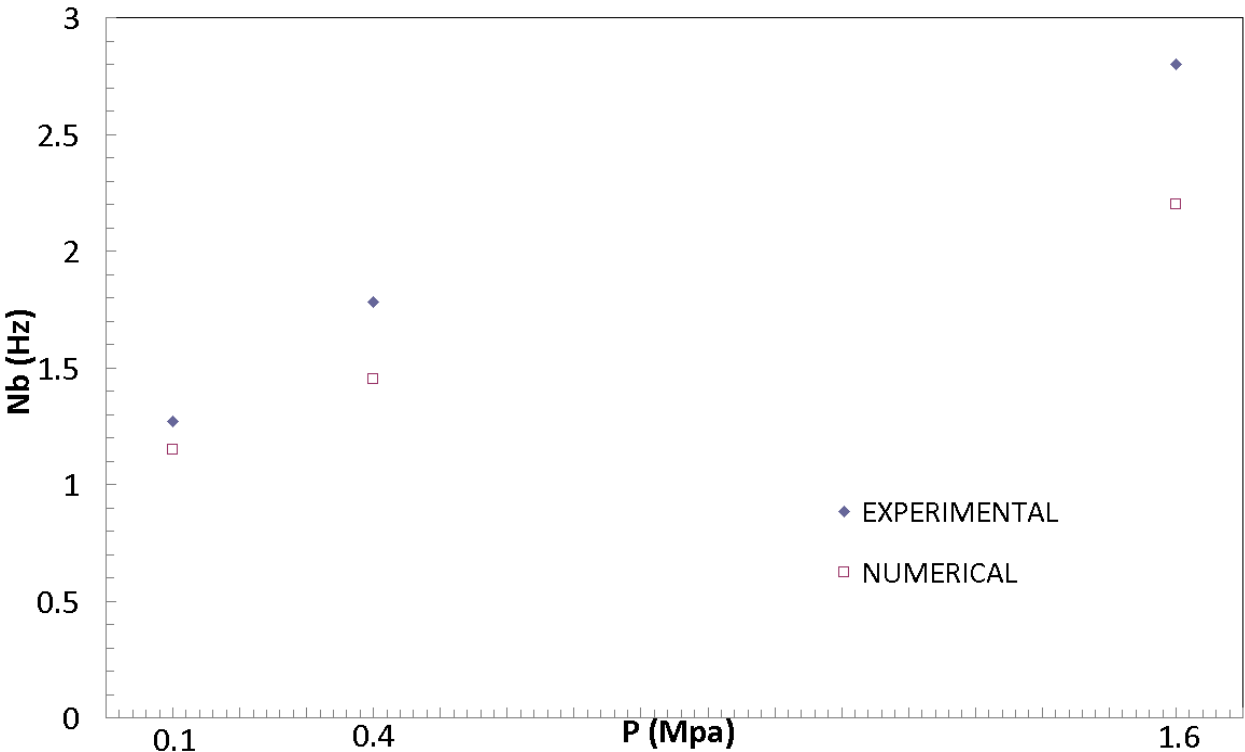
Fig. 13. Nb versus pressure, numerical X experimental: no tubes, U_f = 0.6 m/s
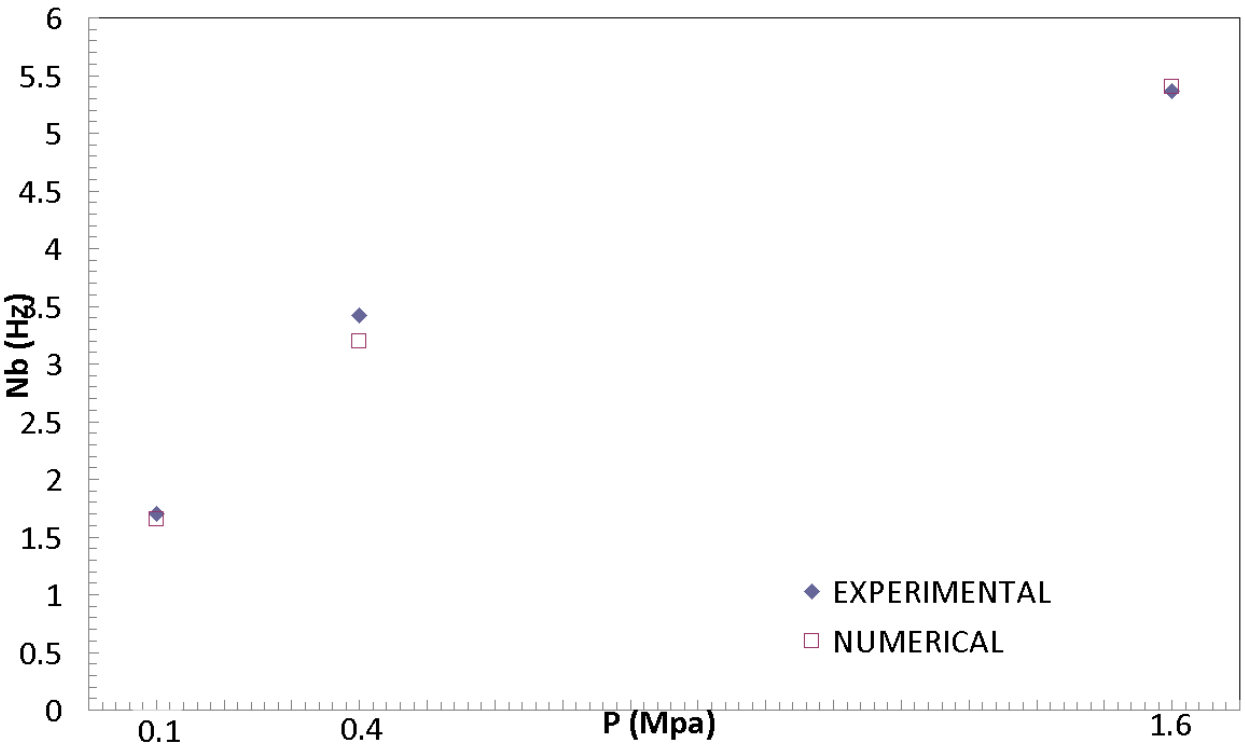
Fig. 14. Nb versus pressure, numerical X experimental: S4 arrangement, U_f = 0.6 m/s

Figure 15 to 18 shows a comparison for the mean bubble velocity. In all cases, the simulated results are underestimated in relation to the experiments. However, the trend observed for the experimental results with a maxima around 0.4 MPa is verified for the numerical results for all the tube arrangements. For the bed without tubes the experimental increase trend of Vb with pressure is valid for pressures higher than 0.4 MPa.
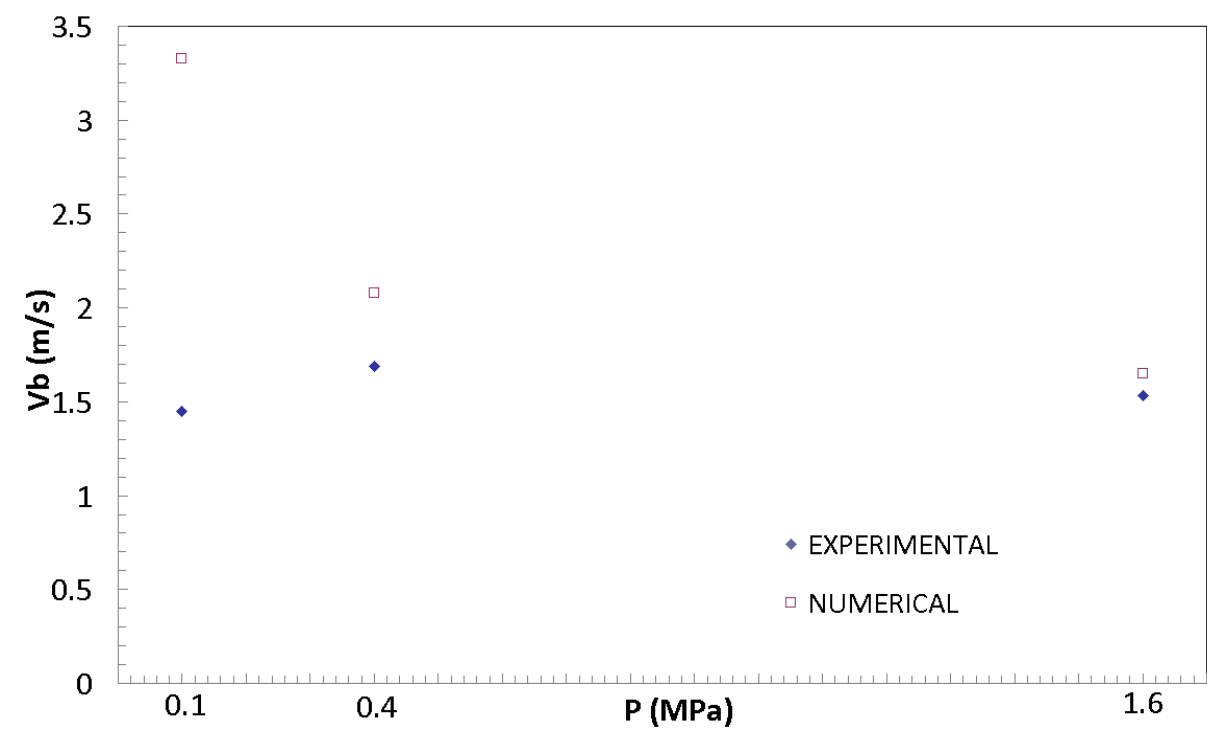
Fig. 15. Vb versus pressure, numerical X experimental: : I4 arrangement, U_f = 0.6 m/s

Fig. 16. Vb versus pressure, numerical X experimental: S4D arrangement, U_f = 0.6 m/s

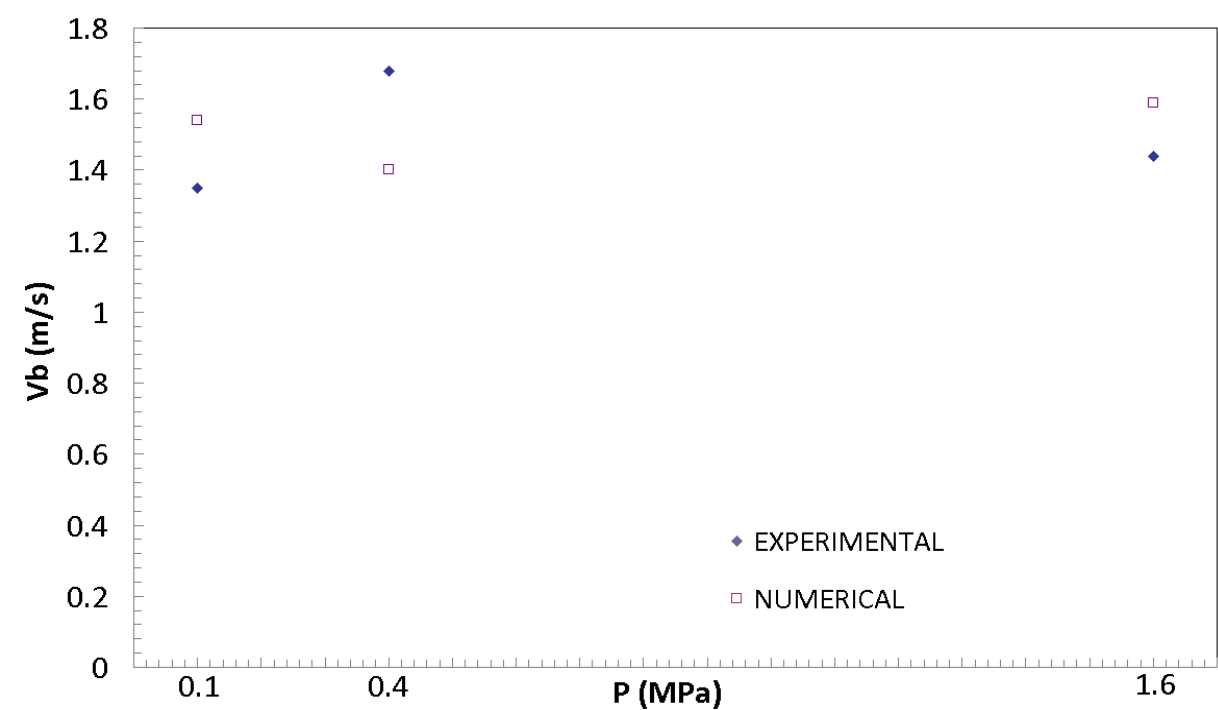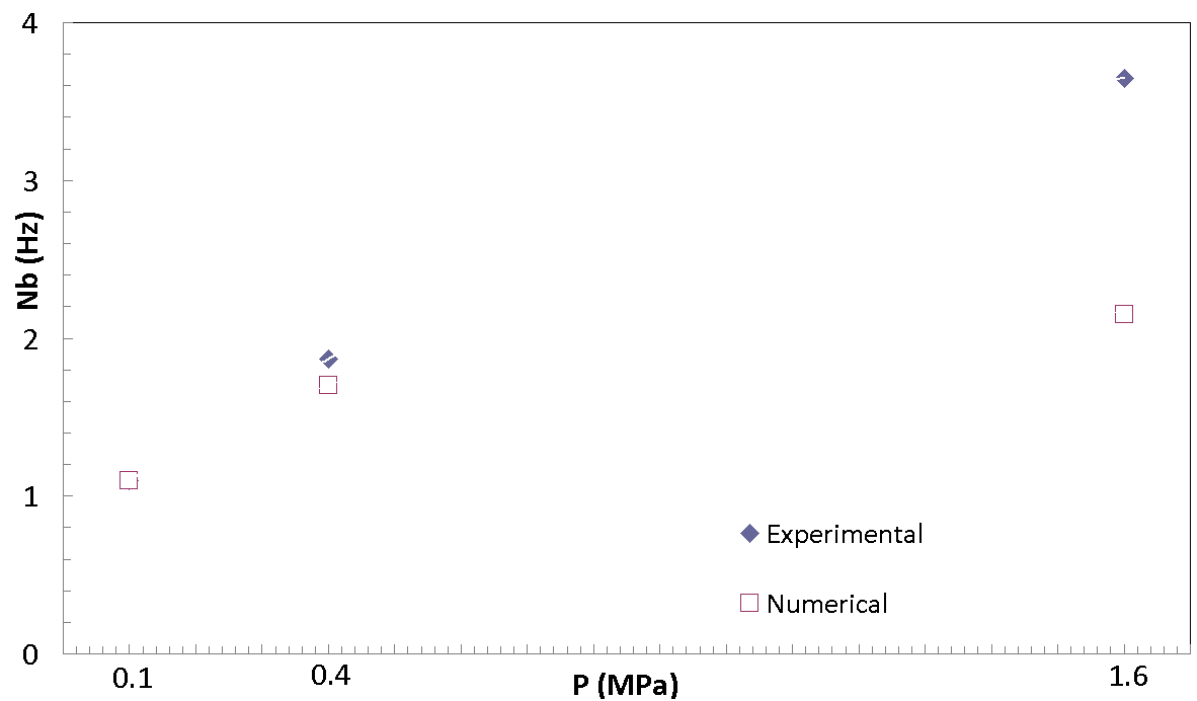Fig. 17. Vb versus pressure, numerical X experimental: : no tubes, U_f = 0.6 m/s

Fig. 18. Vb versus pressure, numerical X experimental: : S4 arrangement, U_f = 0.6 m/s

Figures 19 and 20 shows a comparison for the bubble frequency for U_f = 0.2 m/s. Comparison with results in Figs. 12 and 14 shows that the numerical results, although smaller are closer to the experimental. The tendency holds true for both S4 and S4D arrangements. Comparison with the numerical results for the S4D and S4 arrangements

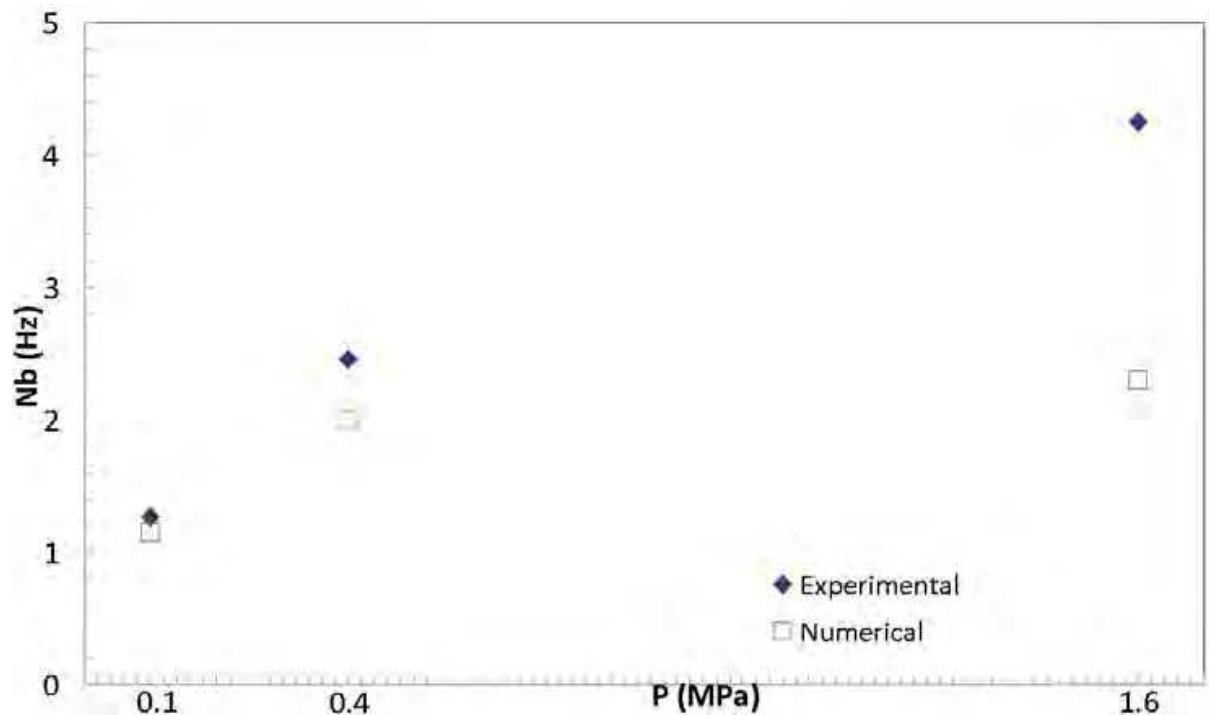Fig. 19. Nb versus pressure, numerical X experimental: : S4 arrangement, U_f = 0.2 m/s

Fig. 20. Nb versus pressure, numerical X experimental: S4D arrangement, U_f = 0.2 m/s

given in Fig. 6 and 7, also shows that Nb increases with increasing excess velocity. The last, is the same drift verified for the experimental values.

Figures 21 and 22 present the results for the time averaged kinetic energy dissipation as a function of circumferential position θ on the tube surface for the S4 arrangement for two distinct pressures. As it would be seen the highest experimental results are between 90 and
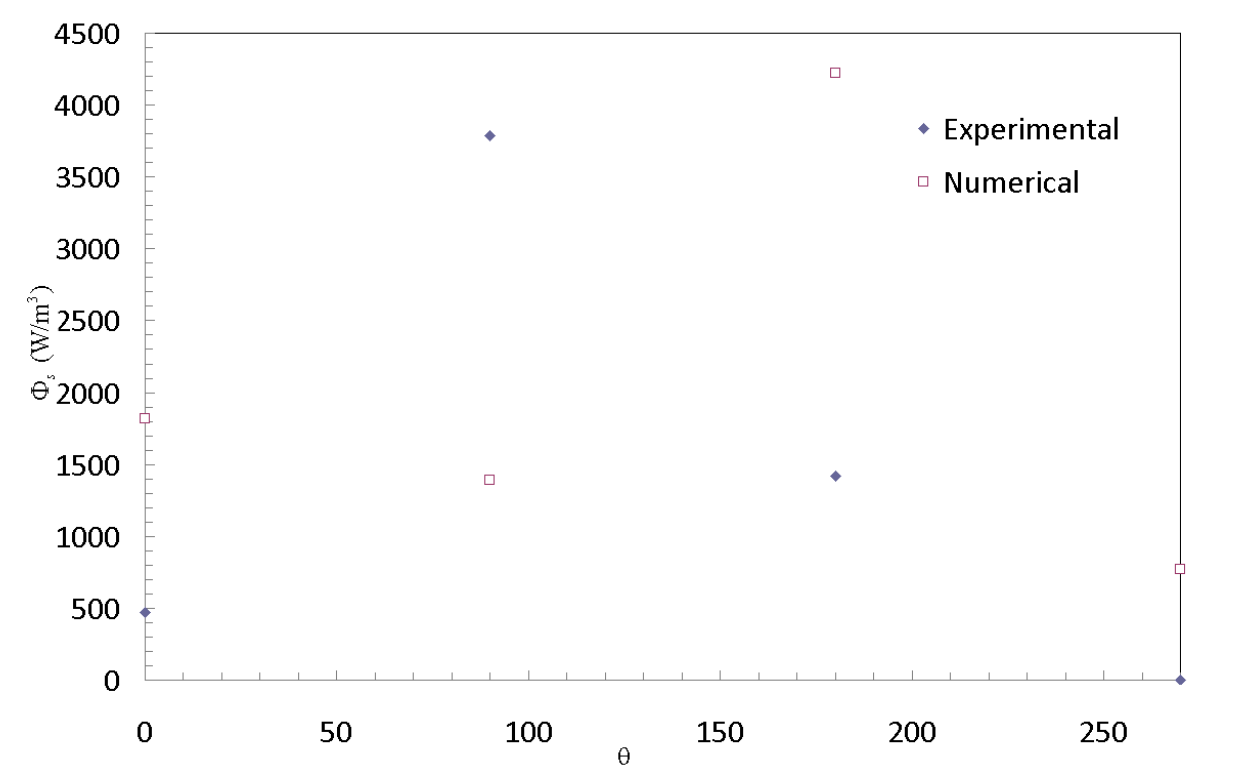
Fig. 21. Time averaged kinetic energy dissipation predicted for different tube arrangements at two different operating pressures: : S4 arrangement, P = 0.1 MPa
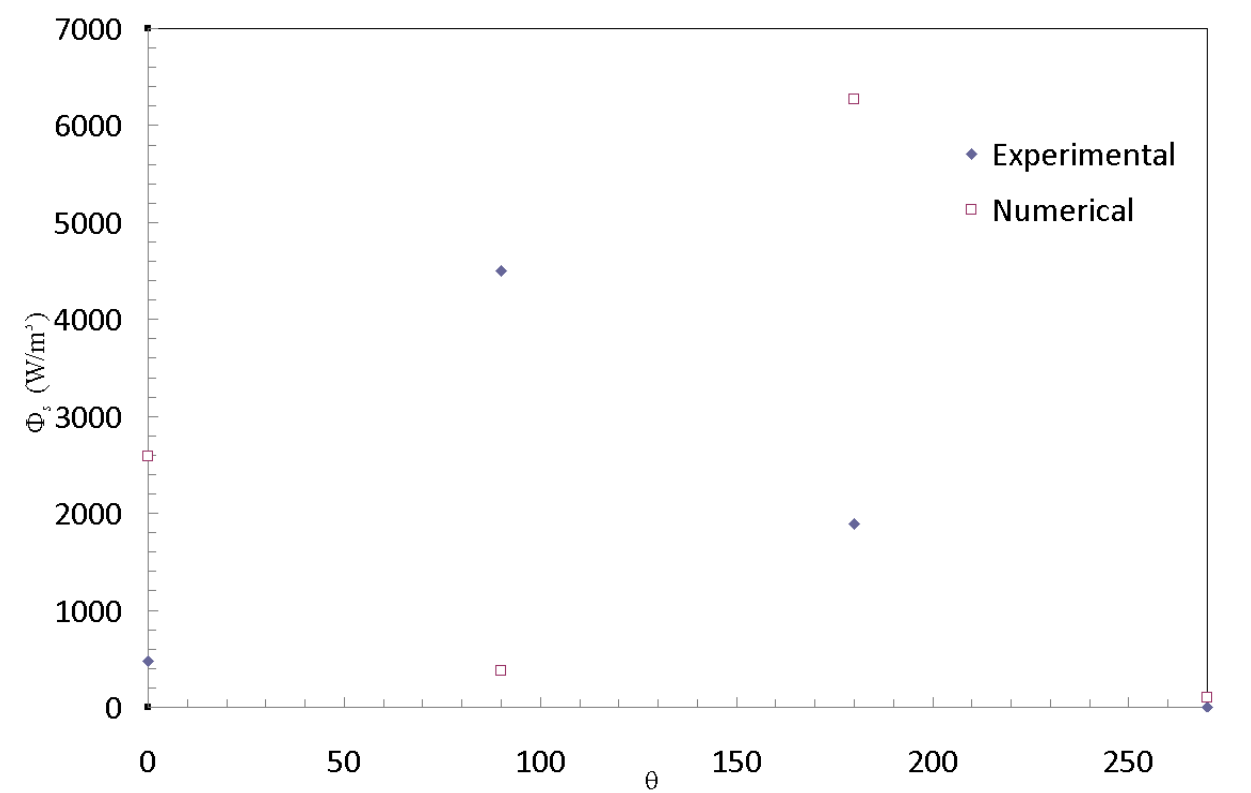

Fig. 22. Time averaged kinetic energy dissipation predicted for different tube arrangements at two different operating pressures : : S4 arrangement, P = 1_6 MPa

240 degrees, while for the numerical are between 30 and 150. The numerical values are over predicted in the range 0 to 100 degrees and above 240 degrees. In the range from 100 to 240 degrees the numerical are below the experimental. Similar trends are verified for the 1.6 MPa pressure, with the experimental curves less sensitive to pressure variation . By his turn the numerical values, show more sensitivity to pressure, although with the same magnitude order.

5. Conclusion

In this work was investigated numerically the hydrodynamics of two dimensional beds with immersed tubes. The simulations were based on an experimental bed with different tube bank geometries, operating pressures and gas excess velocities. The objective of this study was two fold: explore and investigate some effects not previously explored in the literature, to verify the feasibility of the MFIX code for such a kind of study.

The simulation's results were framed in terms of averaged solids kinetic energy dissipation rate and bubble parameters (frequency and mean velocity). A comparison between the numerical results for frequency and the experiments shows good agreement for low pressures. Also, some similar drifts were identified, e.g., greater frequency for greater excess velocities. By his turn, the bubble velocity numerical results agrees better with experiments for high pressures. For the bed with tubes, a maxima of bubble velocity for intermediate pressure is identifiable, this could not be verified for the numerical results. Our results points to significant influences in the predicted dissipation rates and consequently, in the erosion rate, when employing different drag models. The dissipation rate is also influenced by either the use of blending functions for the transition between the plastic and viscous regime of solids flow or the use of a constant viscosity model. The results are key sensitive to the slip condition for the gas phase in the surface of the tube. In the case of a free slip condition for the gas phase the lowest values of dissipation are obtained By his turn, for the solids kinetic dissipation energy, the range of angles that gives maximum values are shifted in relation to the experiments. Finally, remarks towards better agreement with experimental values can also be done for the energy dissipation model. Specifically, according to the monolayer erosion model and its discussion above Eq. (19) some degree of uncertainty is associated to the multiplying constant, as the exact value of elasticity of collision is not known.

6. References

Achim, D., Easton, A. K., Schwarz, M. P., Witt, P.J., Zakhari, A., 2002, "Tube erosion modelling in a fluidised bed", Applied Mathematical Modelling, Vol 26, pp. 191-201.

Almstedt, A. E., 1987, A study of bubble behaviour and gas distribution in pressurized fluidized beds burning coal. Thesis for the degree of Licentiate of Engineering, Chalmers University of Technology, Goteborg. Sweden.

Anderson, T. B., 1967, "A fluid mechanical description of fluidized beds: Equations of motion", Industrial Engineering Chemical Fundamentals, Vol 6, pp. 527-539.

Benyahia, S., 2008, "Validation study of two continuum granular frictional flow theories", Industrial Engineering Chemical Research, 47, 8926-8932.

Benyahia, S., Syamlal, M., O'Brien, T. J., "Summary of MFIX Equations 2005-4", 1 March 2006, Available from
  http://www.mfix.org/documentation/MfixEquations2005-4-1.pdf.

Benyahia, S., Syamlal, M., O'Brien, T. J., 2006, "Extension of Hill–Koch–Ladd drag correlation over all ranges of Reynolds number and solids volume fraction", Powder Technology, 162, 166-174.

Bouillard, J. X., Lyczkowski, R. W., 1991, "On the erosion of heat exchanger tube banks in fluidized-bed combustor", Powder Technology, Vol 68, pp. 37-51.

Cebeci, T., Shao, J. P., Karyeke, F., Laurendeau, E., 2005, Computational Fluid Dynamics for Engineers, Horizon Publishing Inc, USA, 402p.

Dietiker, J., "Cartesian Grid User Guide", 4 September 2009, Available from
  https://mfix.netl.doe.gov/documentation/Cartesian_grid_user_guide.pdf.

Enwald, H., Peirano, E., Almstedt, A. E., Leckner, B., 1999, "Simulation of the fluid dynamics of a bubbling fluidized bed: Experimental validation of the two-fluid model and evaluation of a parallel multiblock solver", Chemical Engineering Science, 54, 311-328.

Ergun, S., 1952, "Fluid-flow through packed columns", Chemical Engineering Progress, Vol 48, n. 2, pp. 91-94.

Fan, J. R., Sun, P., Chen, L. H., Cen, K. F., 1998, "Numerical investigation of a new protection method of the tube erosion by particle impingement", Wear, Vol 223, pp. 50-57.

Gustavsson, M., Almstedt, A. E., 1999, "Numerical simulation of fluid dynamics in fluidized beds with horizontal heat exchanger tubes", Chemical Engineering Science, 55, 857-866.

Gustavsson, M., Almstedt, A. E., 2000, "Two-fluid modelling of cooling-tube erosion in a fluidized bed", Chemical Engineering Science, 55, 867-879.

He, Y. R., Lu, H. L., Sun, Q. Q., Yang, L. D., Zhao, Y. H., Gidaspow, D., Bouillard, J., 2004, "Hydrodynamics of gas-solid flow around immersed tubes in bubbling fluidized beds", Powder Technology, 145, pp. 88-105.

He, Y. R., Zhan, W., Zhao, Y., Lu, H. Schlaberg, I., 2009, "Prediction on immersed tubes erosion using two-fluid model in a bubbling fluidized bed", Chemical Engineering Science, 64, pp. 3072-3082.

Kobayashi, N., Yamazaki, R., Mori, S., 2000, "A study on the behaviour of bubbles and solids in bubbling fluidized beds", Powder Technology, Vol 113, pp. 327-344.

Lathowers, D., Bellan, J., 2000, "Modeling of dense gas-solid reactive mixtures applied to biomass pyrolysis in a fluidized bed", Proceedings of the 2000 U.S. DOE Hydrogen Program Review, NREL/CP-570-28890. USA.

Lee, S. W., Wang, B. Q., 1995, "Effect of particle-tube collision frequency on material wastage on in-bed tubes in the bubbling fluidized bed combustor", Wear, Vol 184, pp. 223-229.

Lyczkowski, R. W., Bouillard, J. X., 2002, "State-of-the-art review of erosion modeling in fluid/solid systems", Progress in Energy and Combustion Science, Vol 28, pp. 543-602.

Ozawa, M., Umekawa, H., Furui, S., Hayashi, K., Takenaka, N., 2002, "Bubble behavior and void fraction fluctuation in vertical tube banks immersed in a gas-solid fluidized-bed model", Experimental Thermal and Fluid Science, Vol 26, pp. 643-652.

Pannala, S., Daw, C. S., Finney, C. E. A., Benyahia, S., Syamlal, M., O´Brien, T. J., "Modelling the collisional-plastic stress transition for bin discharge of granular material", 2009, Powders and Grains 2009 – Proceeding of the 6th International Conference on Micromechanics of Granular Media, pp. 657-660.

Schaeffer, D. G., 1987, "Instability in the evolution equations describing incompressible granular flow", Journal Differential Equations, v. 66, pp. 19-50.

Siravastava, A., Sundaresan, S., 2003, "Analysis of a frictional–kinetic model for gas–particle flow", Powder Technology, v. 129, pp. 72-85.

Syamlal, M., 1998, "MFIX Documentation, Numerical Techniques", Technical Note, DOE/MC-31346-5824, NTIS/DE98002029, National Technical Information Service, Springfield, VA, USA.

Syamlal, M., Rogers, W. A., O'Brien, T. J., 1993, "MFIX Documentation, Theory Guide", Technical Note, DOE/METC-94/1004, NTIS/DE94000087, National Technical Information Service, Springfield, VA, USA.

Wang, J., van der Hoef, M. A., Kuipers, J. A. M., 2010,"CFD study of the minimum bubbling velocity of Geldart A particles in gas-fluidized beds", Chemical Engineering Science, 65, pp. 3772-3785.

Wen, C. Y., Yu, Y. H., 1966, "Mechanics of Fluidization", Chemical Engineering Progress Symposium Series, Vol 62, n. 62, pp. 100-111.

Wiman, J., 1994, An experimental study of hydrodynamics and tube erosion in a pressurized fluidized with horizontal tubes. Thesis for the degree of Licentiate of Engineering, Chalmers University of Technology, Goteborg. Sweden.

Wiman, J., Almstedt, A. E., 1997, "Hydrodynamics, erosion and heat transfer in a pressurized fluidized bed: influence of pressure, fluidization velocity, particle size and tube bank geometry", Chemical Engineering Science, Vol 52, pp. 2677-2695.

Wong, Y. S., Seville, J. P. K., 2006, "Single-particle motion and heat transfer in fluidized beds", AIChe Journal, Vol 52, pp. 4099-4109.
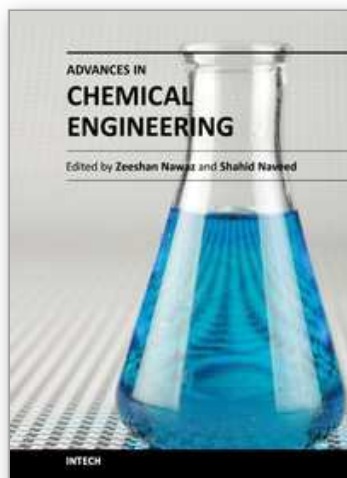
Advances in Chemical Engineering

Edited by Dr Zeeshan Nawaz

Chemical engineering applications have been a source of challenging optimization problems in terms of economics and technology. The goal of this book is to enable the reader to get instant information on fundamentals and advancements in chemical engineering. This book addresses ongoing evolutions of chemical engineering and provides overview to the sate of the art advancements. Molecular perspective is increasingly important in the refinement of kinetic and thermodynamic molding. As a result, much of the material was revised on industrial problems and their sophisticated solutions from known scientists around the world. These issues were divided in to two sections, fundamental advances and catalysis and reaction engineering. A distinct feature of this text continues to be the emphasis on molecular chemistry, reaction engineering and modeling to achieve rational and robust industrial design. Our perspective is that this background must be made available to undergraduate, graduate and professionals in an integrated manner.

How to reference

In order to correctly reference this scholarly work, feel free to copy and paste the following:

A.M.S. Costa, F.C. Colman, P.R. Paraiso and L.M.M. Jorge (2012). CFD Modelling of Fluidized Bed with Immersed Tubes, Advances in Chemical Engineering, Dr Zeeshan Nawaz (Ed.), ISBN: 978-953-51-0392-9, InTech, Available from: http://www.intechopen.com/books/advances-in-chemical-engineering/cfd-modelling-of-fluidized-bed-with-imersed-tubes

INTECH
open science | open minds